arXiv:2406.03176v1 [cs.CV] 5 Jun 2024

MMCL: Boosting Deformable DETR-Based Detectors with Multi-Class Min-Margin Contrastive Learning for Superior Prohibited Item Detection

Mingyuan Li, Tong Jia*, Hui Lu, Bowen Ma, Hao Wang, Dongyue Chen
Northeastern University

Abstract

Prohibited Item detection in X-ray images is one of the most effective security inspection methods. However, differing from natural light images, the unique overlapping phenomena in X-ray images lead to the coupling of foreground and background features, thereby lowering the accuracy of general object detectors. Therefore, we propose a Multi-Class Min-Margin Contrastive Learning (MMCL) method that, by clarifying the category semantic information of content queries under the deformable DETR architecture, aids the model in extracting specific category foreground information from coupled features. Specifically, after grouping content queries by the number of categories, we employ the Multi-Class Inter-Class Exclusion (MIE) loss to push apart content queries from different groups. Concurrently, the Intra-Class Min-Margin Clustering (IMC) loss is utilized to attract content queries within the same group, while ensuring the preservation of necessary disparity. As training, the inherent Hungarian matching of the model progressively strengthens the alignment between each group of queries and the semantic features of their corresponding category of objects. This evolving coherence ensures a deep-seated grasp of category characteristics, consequently bolstering the anti-overlapping detection capabilities of models. MMCL is versatile and can be easily plugged into any deformable DETR-based model with dozens of lines of code. Extensive experiments on the PIXray and OPIXray datasets demonstrate that MMCL significantly enhances the performance of various state-of-the-art models without increasing complexity. The code has been released at https://github.com/anonymity0403/MMCL.

1 Introduction

Prohibited item detection in X-ray images is an essential security inspection measure extensively utilized in airports, postal services, government departments, and border control. The current mainstream method involves using security screening machines to perform X-ray transmission imaging on packages, which are then inspected by professionally trained security personnel. As computer vision technology evolves, increasingly more researchers are attempting to adapt general domain techniques, such as image classification, object detection, and semantic segmentation, to assist security personnel in their inspection tasks, thereby mitigating potential safety risks due to human negligence. However,

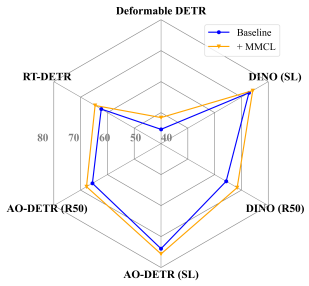

Figure 1: Generalization analysis.

*Corresponding author

Preprint. Under review.

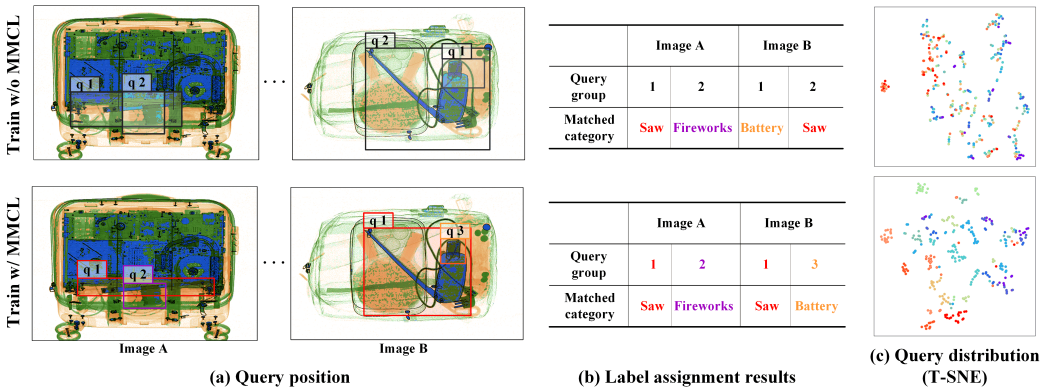

Figure 2: Comparison between queries trained without MMCL and queries trained with MMCL. For clarity, only one query from each query group is displayed, where 'q n' in (a) represents the current query from query group n. (a) shows the predicted results of the queries in images A and B. (b) displays the true label categories to which each query has been assigned. (c) presents a 2D comparison chart of the queries after T-SNE dimensionality reduction, where points of the same color represent queries from the same group.

as depicted in Fig. 2 (a), X-ray images exhibit an abundance of overlapping phenomena, leading to the entanglement of foreground and background information. Consequently, targeted improvements to general object detectors are advantageous for enhancing the precision of the models' detection capabilities.

Currently, there are two main solutions to address overlapping phenomena in X-ray images. The precise label assignment approach, represented by IAA [1], LAreg [2], and HSS [3], improves the focus of the model on the foreground information by increasing the Intersection over Union (IoU) value between positive sample boxes and ground-truth boxes. The attention mechanism approach, represented by DAM [4], PDLC [1], and RIA [5], strengthens the model's detection capabilities by capturing category-specific features to align the tasks of detection classification and localization. However, they are limited to the CNN architecture and lack a decoding mechanism to help decouple foreground and background features through the prior knowledge in the queries [6] [7] [8]. Some research, such as DETR [6], Anchor-DETR [9], and Stable-DINO [10], indicates that a clear definition of content query semantics contributes to the enhancement of model performance. AO-DETR [11] expands on this viewpoint by allocating content queries during the training process to extract features of specific category objects and make predictions, demonstrating the viability of clarifying the categorical meanings of content queries. However, this method's process is overly complicated, resulting in low portability.

For deformable DETR-based models, content queries are responsible for providing category semantic priors, while positional queries collaborate to offer positional priors. Theoretically, class-specific content queries and the features of class-specific objects are expected to follow a Gaussian distribution, showcasing a clear gap between features of samples from different classes, while features within the same class are similar yet distinctive. However, as illustrated in Fig. 2 (c), the T-SNE [12] dimensionality reduction distribution of content queries in the baseline model is chaotic, with no apparent class boundaries. At the same time, as shown in Fig. 2 (b), the categories of contraband matched by queries during training are not stable. To address this, we propose the Multi-Class Min-Margin Contrastive Learning (MMCL) mechanism. Firstly, through the Multi-Class Inter-Class Exclusion (MIE) loss, we repel content queries between groups, ensuring that there is sufficient difference among each group of samples. Secondly, through the Intra-Class Min-Margin Clustering (IMC) loss, we attract content queries within the group, making each query similar but distinct. Under the influence of this mechanism, as shown in Fig. 2 (c), the content queries are presented as fifteen clusters of discrete points that mutually repel between groups and attract within groups while maintaining distance. As training progresses, the categories of ground truth objects matched by the queries through label assignment mechanism become more stable, indirectly increasing the number of training samples. As a result, class-specific content queries will master the ability to extract information about specific category foreground items from various scenarios where foreground and

background features overlap, thus ultimately enhancing the model's resilience against overlapping in contraband detection in X-ray images.

Extensive experiments have demonstrated the effectiveness of our approach for most deformable DETR variants. Taking the PIXray [13] dataset as an example, as shown in Fig. 1, the MMCL mechanism can increase the AP of RT-DETR [14] (ResNet-50) increased from 62.3% to 63.6%, AO-DETR [11] (ResNet-50) from 65.6% to 66.8%, and DINO [8] (Swin-L) from 72.8% to 73.2%, among others. Furthermore, experiments on another large-scale X-ray image contraband detection dataset, OPIXray [5], yielded consistent conclusions.

The main three contributions are summarized as follows: Firstly, we reveal that content queries can be linked with category semantic information to enhance the anti-overlapping feature extraction capability of deformable DETR-like models. Secondly, we propose a plug-and-play Multi-Class Min-Margin Contrastive Learning (MMCL) mechanism that, without increasing model complexity, clarifies the category semantic information of content queries to improve model detection performance. Thirdly, MMCL is versatile and applicable to various deformable DETR variants, including RT-DETR, DINO, and AO-DETR. It proves effective on multiple prohibited item datasets and helps these models exceed state-of-the-art (SOTA) performance. Finally, we introduce a metric to measure the label assignment instability between adjacent decoder layers, named layer instability score (LIS), offering a new perspective for the analysis of DETR-like models.

2 Related Work

Prohibited Item Detection. Prohibited item detectors are primarily based on general object detection models that have been improved to address the issue of overlapping phenomena in X-ray images. SIXray [15] introduces a FPN-based method called class-balanced hierarchical refinement, which progressively removes background features at multiple levels. OPIXray proposes a de-occlusion attention module (DOAM) that simultaneously emphasizes the material information and the edge information of prohibited items. Xdet [3] proposes the use of the Otsu [16] algorithm to extract the latent relationship between the area and category of prohibited items to align the classification and localization tasks. GADet [1] points out that the diagonal length is more stable and has greater discriminative power and has designed a physical diagonal length constraint strategy to train the model for both classification and localization tasks. AO-DETR [11] introduces a DETR-like model to the field of prohibited item detection for the first time, proposing a look forward densely mechanism for accurate localization of the boundaries of prohibited items, and introduces Category-Specific One-to-One Assignment to add explicit category meaning to object queries, enhancing the decoder's ability to extract specific category foreground features from overlapping features.

DETR-like object detectors. Since the DEtection TRansformer (DETR) was proposed, end-to-end object detectors based on the transformer architecture have developed rapidly. Thanks to the one-to-one matching mechanism, the model does not need to use anchors with hyperparameters or Non-Maximum Suppression (NMS) post-processing. However, the convergence speed of the model is extremely low. There are two mainstream approaches to enhancing the convergence rate of models. One approach involves improving the label assignment process by introducing more supervisory information or enhancing the quality of the existing supervisory information to bolster the model's ability to represent features. H-DETR [17], DAC-DETR [18], and Co-DETR [19] maintain the one-to-one label assignment characteristic of DETR while incorporating one or multiple traditional one-to-many label assignment methods in a hybrid collaborative training scheme. Group-DETR [20] employs K groups of independent self-attention mechanisms, heads, and object queries with one-to-one matching for group-specific training, thus introducing more supervisory signals to optimize the modules with shared parameters. Stable-DINO [10] emphasizes the positional relationship between positive samples and ground truth as a supervisory signal to improve the quality of training. The other approach involves a deeper understanding of the role of queries within the DETR framework. Deformable DETR [21] utilizes the top-K predicted reference boxes obtained by the encoder as priori information of queries in the decoder. Anchor-DETR and DAB-DETR [7] introduce the randomly initialized anchor embeddings and positional encoding them as the positional query to assist the content query in extracting features of targets of specific sizes. DINO employs a mixed query selection strategy, initializing anchor boxes solely with the positional information corresponding to the top-K features selected, while maintaining the content queries in their original static state, akin to

DAB-DETR. AO-DETR enhances the model's ability to handle object occlusions by designing rules for label assignment that constrain the object category each query identifies during training.

Contrastive learning. Contrastive learning is an effective method for pulling close sample pairs within the same class and pushing away the sample pairs between different classes. Broadly, it can be categorized into self-supervised contrastive learning and supervised contrastive learning. Self-supervised contrastive learning can be divided into two categories: one is instance-wise contrastive learning, which includes SimCLR [22] and MoCo [23]. The former involves treating two data augmentations of the same instance as intra-class samples and augmentations of different instances as inter-class samples. The latter is cluster-based contrastive learning, which includes methods like CC [24] and TCL [25]; this approach generates pseudo-labels for categories using some clustering algorithms and then provides them to a supervised contrastive learning framework. Supervised contrastive learning can be categorized into three mainstream paradigms. The first is based on the Triplet loss [26], which includes the triplet loss and N-pair loss. The second is based on the Softmax function, encompassing methods such as AM-Softmax [27], Circle loss [28], and SupCon loss [29]. The third is based on the Cross-Entropy loss, exemplified by EBM [30] and C2AM [31].

3 Proposed Method

3.1 Explore the Significance of Clarifying the Category Meaning of the Content Queries:

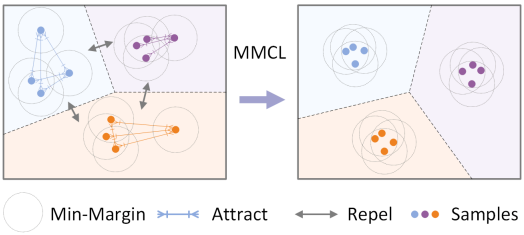

Figure 3: MMCL can repel samples between categories while attracting samples within the same category. When the similarity between samples within a category exceeds the Min-Margin, it ceases the attraction to preserve the necessary diversity of intra-class samples. The color of points represents their category.

In this part, we analyze the role of content queries in the decoder of models based on deformable DETR, and then elucidate why we engage in contrastive learning for content queries according to the number of categories. Given an image, the backbone and encoder extract the mulit-scale spatial feature $X \in \mathbb{R}^{N \times C}$, and predict a group of proposals including classification results C and localization results $R \in \mathbb{R}^{N \times 4}$. Taking the decoder's match part of DINO as an example, in a two-stage approach, the top N_{pred} localization results with the highest classification confidence predicted by the encoder are used as reference boxes $R^0 \in \mathbb{R}^{N_{pred} \times 4}$, where N_{pred} is the same as the number of queries. Content queries $Q_c^0 \in \mathbb{R}^{N_{pred} \times C}$ is randomly initialized, represented as $Q_c^0 = \text{Embedding}(N_{pred}, C)$ Positional queries are implicitly included in Equation 1, responsible for providing prior positional information. For more details, please refer to Appendix A. The decoder is then responsible for further feature extraction from X with reference boxes and query pairs by L decoder blocks, which includes self-attention, deformable attention, and linear mapping layers, to predict the final results. Overall, the decoder block of the l-th layer can be simplified as follows:

$$Q_c^{l+1}, R^{l+1}, C^{l+1} = \mathcal{D}^l(Q_c^l, R^l, X; \theta^l). \tag{1}$$

Content queries provide direct information for classification and localization, whereas positional queries primarily assist in delivering prior knowledge of positioning. Therefore, theoretically, if we can decouple various potential semantic features of categories in content queries and retain the semantic features of one category, then its detection capability for items of that category will be enhanced.

3.2 Multi-Class Min-Margin Contrastive Learning (MMCL)

We propose an MMCL mechanism that can group and cluster content queries of any decoder layer according to the number of categories K, as shown in Fig. 3. MMCL comprises two loss functions: Multi-Class Inter-Class Exclusion (MIE) and Intra-Class Min-Margin Clustering (IMC), which are respectively responsible for the repulsion of samples between groups and the attraction of samples

within groups. Their mathematical expressions are as follows:

$$L_{MMC}(Q,K) = \gamma L_{IMC}(Q,K) + \eta L_{MIE}(Q,K), \tag{2}$$

wherein γ and η are two weighting parameters used to balance the proportion of the two losses. Related ablation experiments can be found in Section 4.

MIE loss. Specifically, the MIE loss utilizes the cosine similarity of inter-group samples to calculate the mean cross-entropy loss, thereby suppressing the similarity of inter-group samples. Its formula is as follows:

$$L_{MIE}(Q,K) = \frac{-1}{K(K-1)n^2} \sum_{k_1=1}^{K} \sum_{k_2=1}^{K} \sum_{i=1}^{n} \sum_{j=1}^{n} \mathbb{1}[k_1 \neq k_2] log(1 - s_{i,j}^{k_1,k_2}), \tag{3}$$

where $\mathbb{1}[k_1 \neq k_2] \in \{0,1\}$ represents an indicator function. It equals 1 if $k_1 \neq k_2$, and 0 in all other cases. n is the number of samples for each group of content queries, which is the quotient of the total number of samples N_{pred} and the number of categories of the dataset K. In addition, $s_{i,j}^{k_1,k_2}$ is the cosine similarity between the i-th sample of the k_1-th group, and j-th sample of the k_2-th group. When the similarity of two intra-class samples is high, *i.e.*, $s_{i,j}^{k_1,k_2} \to 1$, then $L_{MIE} \to +\infty$. This means the loss will suppress the similarity between inter-class samples. Ultimately, as the gradient is back-propagated, the parameters between samples are updated, causing $s_{i,j}^{k_1,k_2} \to 0$.

IMC loss. In addition, the ideal content queries for a single category should remain similar but distinct. For the attraction of intra-group sample pairs, the ideal content queries of one category should be similar but distinct. In order to attract samples within the same group while still maintaining the necessary level of distinctiveness, we propose an intra-class clustering loss function with a minimum margin, as follows:

$$L_{IMC}(Q,K) = \frac{-1}{\Sigma \mathcal{M}_{i,j}^k} \sum_{k=1}^{K} \sum_{i=1}^{n} \sum_{j=1}^{n} \mathcal{M}_{i,j}^k \left[w_{i,j}^k \cdot log(s_{i,j}^{k,k}) \right], \quad \mathcal{M}_{i,j}^k = \begin{cases} 1, & w_{i,j}^k \cdot log(s_{i,j}^{k,k}) \geq m \\ 0, & w_{i,j}^k \cdot log(s_{i,j}^{k,k}) < m \end{cases} \tag{4}$$

Where $w_{i,j}^k = exp(-\alpha \cdot rank(s_{i,j}^{k,k}))$ is used to weight the loss value based on the similarity ranking among intra-group sample pairs, which can amplify the loss values of the similar pairs and speed up the training [31]. $\mathcal{M} \in \mathbb{R}^{K \times n \times n}$ is a mask, whose element becomes 0 when the weighted similarity loss of sample pair, $w_{i,j}^k \cdot log(s_{i,j}^{k,k})$, falls below the specified intra-class min-margin m. The ICM loss only applies an attractive force to sample pairs whose weighted similarity loss is greater than m. The larger the value of m, the more tolerance there is for diversity among samples within the same class. Since $w_{i,j} \leq 1$, when any $log(s_{i,j}^{k,k}) < m$, the L_{IMC} achieves the global optimum and its value is 0.

3.3 Plug MMCL Mechanism into the Target Decoder Layers

Algorithm 1 Plug MMCL into the Decoder.

Require:
Constant K; Set L, $\hat{L}$, Q_c, P, G;
Ensure:
Initialize the total loss $\mathcal{L}$ to 0;
for $\forall$ decoder layer index $l \in L$ **do**
$\{P_i^l; G_i\} \leftarrow \mathcal{H}^l(P^l, G)$;
$\mathcal{L}^l \leftarrow L_{BASE}(\{P_i^l; G_i\})$;
if $l \in \hat{L}$ **then**
$\mathcal{L}^l \leftarrow \mathcal{L}^l + L_{MMC}(Q_c^l, K)$;
end if
$\mathcal{L} \leftarrow \mathcal{L} + \mathcal{L}^l$;
end for
update networks and Q_c to minimize $\mathcal{L}$;
return Q_c;

MMCL can be seamlessly integrated into deformable DETR-like models without any modifications to the architecture of models, as outlined in Algorithm 1. Given the number of clustering categories K, content queries of all decoder layers Q_c, prediction results of all decoder layers P, ground truth set G, and the set of layers $\hat{L}$ which need contrastive learning, we iterate over the decoder layer set L. For each layer l, based on the results of the Hungarian label assignment mechanism $\mathcal{H}^l$ [6], we obtain the one-to-one relationship between prediction results and ground truth set. Furthermore, through the inherent decoder loss function L_{BASE}, we obtain the loss $\mathcal{L}^l$ of l-th layer. The inherent decoder loss function L_{BASE} can calculate the loss of the l-th layer using the matched predicted values and

ground true values. Then, we ascertain whether the current layer l is included in the set $\hat{L}$. If it is, we obtain the MMCL loss for the current layer by inputting the content queries Q_c^l of the current layer and the number of categories K into Equation 2. And then we add it to the loss of the current layer to calculate the sum. Finally, the model utilizes the sum of loss of each layer, denoted as $\mathcal{L}$, to update the model parameters as well as the content queries of all layers.

Consequently, this facilitates the refinement of similarity for the content queries of target layer. Under the influence of our MMCL mechanism, as training progresses, from the perspective of feature distribution, the average distance between one sample and other samples within the same category k_1 will be significantly smaller than the distance between one sample of category k_1 and the samples of category k_2, which can be mathematically represented as:

$$\frac{1}{n-1}\sum_{j}^{n-1} s_{i,j}^{k_1,k_1} \ll \frac{1}{n}\sum_{j}^{n} s_{i,j}^{k_1,k_2}, \quad \text{where } i \neq j. \tag{5}$$

Initially, the semantic features of each group of content queries are disordered and ineffective. After the MMCL mechanism is applied, each group of content queries tends to randomly favor an object of a certain category. The Hungarian matching algorithm will match each prediction result with a globally optimal ground true object, thereby guiding the corresponding content query to learn category semantic features. As the training progresses, a group of content queries becomes increasingly accurate in predicting objects of a specific category, which in turn makes the Hungarian matching more inclined to train them to detect objects of the class. This positive feedback enables the content queries within one group, facing different overlapping background interferences, to be trained to detect objects of the same category, ultimately endowing them with strong anti-overlapping capabilities of feature extraction. It is noteworthy that since the number of groups of content queries matches the number of object categories in the dataset, each category of objects will train a group of class-specific content queries proficient in extracting their semantic features.

3.4 Analyze the Effect of the MMCL Mechanism on the Stability of Label Assignment

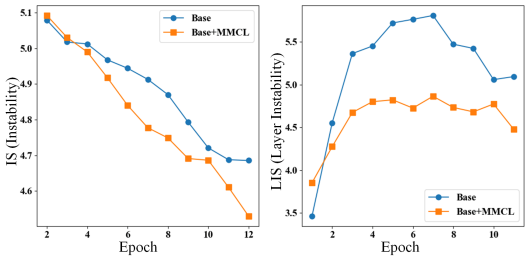

Figure 4: Instability analysis

In order to measure the impact of MMCL on the stability of label assignment in different layers during training, we propose a metric, named Layer Instability Score (LIS). Given a training image, the model will obtain N_{pred} prediction results in the l-th layer decoder on the j-th epoch, which can be denoted as $P^{j,l} = \{P^{j,l}, P^{j,l}, \ldots, P^{j,l}_{N_{pred}-1}\}$. In addition, the ground truth set can be expressed as $G = \{G_0, G_1, \ldots, G_{N_{gt}-1}\}$. Ultimately, we define a metric capable of reflecting the instability of label assignment between adjacent layers, termed the Layer Instability Score (LIS), expressed as follows:

$$LIS^j = \sum_{l=1}^{L}\sum_{n=0}^{N_{pred}} \mathbb{1}(V_n^{j,l} \neq V_n^{j,l-1}), \quad V_n^{j,l} = \begin{cases} m, & \text{if } P_n^{j,l} \text{ matches } G_m \\ -1, & \text{if } P_n^{j,l} \text{ matches nothing} \end{cases} \tag{6}$$

where $V_n^{j,l}$ represents the ground truth label indices assigned to the prediction results of the content queries in the l-th layer during the j-th iteration. The instability for epoch j across the entire dataset is calculated as the mean of the instability values for each image. To ensure clarity of expression, the image index is omitted in Equation 6. LIS takes into account the instability of label assignment between layers, with a lower value indicating greater stability.

In order to comprehensively analyze the impact of the MMCL model training process, we use the IS [32] metric in conjunction with our LIS metric to analyze the instability of label assignment during model training. IS is an indicator that evaluates the instability of label allocation among content queries across different images; the lower the IS value, the more stable the training process. As shown in Fig. 4 (a), the IS score for the standard deformable DETR model decreases as the number of training epochs increases, and under the influence of MMCL, the IS score of the model

becomes lower. This indicates that the content query undergoes more training for a specific category of objects. Additionally, as illustrated in Fig. 4 (b), the LIS score for models first increase and then decrease, suggesting that multi-layer decoder structures require additional assistance to constrain this layer-to-layer inconsistency. Visually, after the integration of MMCL, the LIS scores generally decline, indicating that the MMCL has enhanced the consistency of the training targets for content queries across layers, and thus increased the utilization efficiency of deeper decoder layers for features extracted by shallower layers.

4 Experiments

In order to analyze the impact of the target layer set plugged into the MMCL mechanism on detection performance, as well as the optimal hyperparameters, we firstly conduct extensive ablation experiments on the large-scale contraband X-ray dataset PIXray. These experiments effectively validate the efficacy of the MMCL module and obtained the optimal hyperparameters. Subsequently, we fully demonstrate on two datasets that the MMCL module can be seamlessly integrated into deformable DETR-like models, and compare the deformable DETR-like models with the current state-of-the-art object detection models after adding the MMCL module. Through this comparison, we proved the effectiveness and universality of our method in the deformable DETR-like models, and that our method surpasses the performance of current state-of-the-art object detection methods.

4.1 Experimental Setup

4.1.1 Datasets and Evaluation Metrics

We conducted experiments on two large-scale contraband X-ray datasets, OPIXray and PIXray, both of which are publicly available datasets in the field of contraband object detection.

For the PIXray dataset, we adopt the COCO evaluation metric. AP represents the average precision of the detector at different IoU thresholds, serving as a metric for overall detection performance. AP_{50} is the AP calculated at a single IoU threshold of 0.5, indicating the precision when the detection boxes overlap significantly with the ground truth boxes. AP_{75} is the AP calculated at a single IoU threshold of 0.75, representing the strict precision when the detection boxes overlap significantly with the ground truth boxes. AP_S, AP_M, and AP_L respectively represent the average precision for small objects, medium-sized objects, and large objects.

For the OPIXray dataset, we adopt the VOC evaluation metric. AP is calculated as the area under the Precision-Recall curve of one category at the IoU threshold of 0.5. The mean average precision (mAP) is then computed as the average AP of all categories. mAP serves as a comprehensive evaluation criterion, effectively representing the accuracy and recall of the detector. It provides a holistic assessment that captures the performance strengths and weaknesses of the detector.

4.1.2 Implementation Details

In order to minimize the influence of experimental equipment on the results, we conducted training and testing on the same computer platform, which is equipped with an NVIDIA GeForce RTX 4090 GPU, an Intel Core i9-13900K central processing unit (CPU), 64GB of memory, Windows 10 operating system, and PyTorch 1.13.1. To reduce the impact of non-parameter factors on the experimental results, we used the pre-trained models from the official MMDetection website, including ResNet-50 and Swin-L. Transformer models like DINO utilized the AdamW optimizer with a learning rate of 0.0001 and weight decay of 0.0001. All models underwent 12 training epochs and used the original training strategy of the models with an image size of 320×320.

4.2 Ablation Study

In this part, we firstly conduct a series of ablation experiments to analyze the impact of the MMCL inserted layer set $\hat{L}$ on detection performance and the optimal set. Subsequently, we perform a compatibility analysis of the impact of MIE and MIC on detection performance. Finally, to obtain the optimal performance, we conduct a step-by-step analysis of the influence of hyperparameters of the MMCL module, including the min-margin m in the IMC loss, and weight γ and η for IMC loss and MIE loss, respectively.

Table 1: Ablation study about the MMCL mechanism on DINO [8] on the PIXray [13] dataset. L means all decoder layers. The superscript '$*$' represents the optimal value of the hyper-parameter.

Method	$\hat{L}$	AP	AP_{50}	AP_{75}
DINO	0	**65.7**	**87.1**	**72.7**
	1	64.5	85.7	71.5
	5	10.2	19.4	9.5
	L	64.9	86.3	72.4

(a) Ablation Study of the target layer set.

Method	MIE	IMC	AP	AP_{50}	AP_{75}
DINO	✗	✗	64.3	86.5	71.0
	✓	✗	65.3 (+1.0)	86.7	72.9
	✗	✓	65.1 (+0.8)	86.7	72.1
	✓	✓	65.7 (+1.4)	87.1	72.7

(b) Ablation study of MIE and IMC results.

m	AP	AP_{50}	AP_{75}
1×10^{-1}	65.7	87.1	72.7
3×10^{-2}	66.2	87.2	73.2
$\mathbf{1 \times 10^{-2}}$	**66.4**	**87.9**	**73.3**
3×10^{-3}	65.9	87.4	73.2
1×10^{-4}	60.0	82.2	66.4

(c) $\gamma = 1$,$\eta = 1$

η	AP	AP_{50}	AP_{75}
2	66.0	87.2	73.1
1	65.7	86.7	72.4
0.5	**66.7**	**87.5**	**74.4**
0.25	65.3	86.9	73.2
0.1	56.2	79.1	63.1

(d) $\gamma = 1$, $m^* = 0.01$

γ	AP	AP_{50}	AP_{75}
5	65.1	86.8	72.3
2	66.6	**88.1**	73.7
1	**66.7**	87.5	**74.4**
0.5	66.5	87.6	74.1
0.2	66.1	87.5	73.6

(e) $\eta^* = 0.5$, $m^* = 0.01$

Ablation study of target layer set $\hat{L}$. As indicated in Table 1a, we initially set the hyperparameter values to $m = 0.1$, $\eta = 1$, $\gamma = 1$. MMCL achieved the highest AP value of 65.7% for the content queries output from the 0-th decoder layer, surpassing the results from inserting MMCL individually into other decoder layers or into all decoder layers L. Inserting MMCL into the shallow decoder layers can help content queries clarify categorical semantic features, which aids the deeper decoder layers in further enhancing feature extraction. However, directly inserting MMCL into deeper layers, such as the 5-th layer, will destroy the originally extracted features that are used for the final prediction, leading to a decrease in model performance.

Ablation study of MIE and IMC. As shown in Table 1b, applying the MIE loss and IMC loss individually to the content queries output from the 0-th decoder layer improves the AP by 1.0% and 0.8%, respectively. This demonstrates their effectiveness. In addition, the concurrent utilization of MIE loss and IMC loss led to a significant increase of 1.4% in the AP of model. This validates the exceptional performance of MMCL and highlights the complementarity of MIE and IMC.

Ablation study of the Hyperparameters of MMCL. Initially, we set default values of $\eta = 1$ and $\gamma = 1$, and varied the value of m to select the optimal m^*. As shown in Table 1c, when $m = 0.01$, the three indicators AP, AP_{50}, and AP_{75} reach their maximum values, which are 66.4%, 87.9%, and 73.3% respectively. Subsequently, we maintain the default $\gamma = 1$, and utilize the optimal $m^* = 0.01$ to find the best η^*. As shown in Table 1d, when $\eta = 0.5$, the three indicators AP, AP_{50}, AP_{75} get their maximum, which are 66.7%, 87.5%, 74.4% respectively. Finally, we utilize the optimal $m* = 0.01$ and $\eta^* = 0.5$ to determine the optimal γ^*. As shown in Table 1e, when $\gamma = 1$, the two indicators AP and AP_{75} reached their maximum values, which were 66.7% and 74.4% respectively. This is overall superior to $\gamma = 2$. In summary, the global optimal values of the three hyperparameters of MMCL are $m^* = 0.01$, $\eta^* = 0.5$, $\gamma^* = 1$.

4.3 Comparison with State-of-the-Art Methods

Generalization. In order to assess the efficacy and generalizability of the MMCL mechanism across various deformable DETR variants, we select four deformable DETR-like models as baselines, including deformable DETR [21], RT-DETR [14], AO-DETR [11], and DINO [8], along with two distinct architectural backbones: ResNet-50 [33] and Swin-L [34], respectively. To ensure fairness, all models were trained over 12 epochs, with each implementation carried out using MMDetection [35]. Additionally, the images were uniformly resized to a dimension of 320×320. As depicted in Table 2, when utilizing the ImageNet [36] pretrained ResNet-50 backbone [37], the incorporation of our MMCL mechanism significantly enhances the AP values of deformable DETR, RT-DETR, DINO, and AO-DETR by increments of 3.8%, 3.3%, 2.4%, and 1.2% on the PIXray dataset respectively, illustrating the broad applicability of our approach. Furthermore, with the ImageNet-pretrained Swin-L backbone [34], MMCL facilitates a notable improvement in the AP for DINO and AO-DETR by 0.4% and 0.7%, respectively, demonstrating the efficacy of our method across diverse architectural

Table 2: Comparison with state-of-the-art general detectors on PIXray.

Method	Backbone	MMCL	FPS	PARAMs	GFLOPs	#queries	AP	AP_{50}	AP_{75}	AP_S	AP_M	AP_L
Faster R-CNN [38]	ResNeXt-101	*	70	59.83M	28.35	*	53.6	82.3	60.8	3.9	37.7	62.7
MASK R-CNN [39]	ResNeXt-101	*	73	60.04M	28.35	*	52.4	81.9	59.4	4.2	36.2	61.3
Cascade R-CNN [40]	ResNet-50	*	61	68.97M	22.37	*	56.5	81.3	63.2	8.0	41.0	65.9
ATSS [41]	ResNet-101	*	66	51.14M	27.82	*	52.8	80.8	60.2	7.0	37.4	63.6
GFLv1 [42]	ResNeXt-101	*	66	50.70M	28.51	*	57.5	82.8	66.0	9.1	42.0	67.4
Deformable DETR [21]	ResNet-50	✗	60	52.14M	13.47	300	44.6	74.2	48.5	9.6	30.0	53.0
Deformable DETR [21]	ResNet-50	✓	60	52.14M	13.47	300	48.4 (+3.8)	76.9	52.3	9.1	34.3	57.5
RT-DETR [14]	ResNet-50	✗	64	42.81M	17.07	60	62.3	85.3	69.9	25.6	48.0	70.9
RT-DETR [14]	ResNet-50	✓	64	42.81M	17.07	60	63.6 (+1.3)	85.9	71.4	24.0	49.9	72.6
DINO [8]	ResNet-50	✗	54	58.38M	26.89	30	64.3	86.5	71.0	19.3	48.9	73.9
DINO [8]	ResNet-50	✓	54	58.38M	26.89	30	66.7 (+2.4)	87.5	74.4	23.5	50.7	75.5
DINO [8]	Swin-L	✗	40	229.0M	156.0	30	72.8	90.0	80.1	38.3	60.4	80.4
DINO [8]	Swin-L	✓	40	229.0M	156.0	30	73.2 (+0.4)	89.7	79.9	37.4	58.9	81.1
AO-DETR [11]	ResNet-50	✗	54	58.38M	26.89	30	65.6	86.1	72.0	23.9	50.7	74.8
AO-DETR [11]	ResNet-50	✓	54	58.38M	26.89	30	66.8 (+1.2)	87.6	74.3	24.1	52.4	75.9
AO-DETR [11]	Swin-L	✗	40	229.0M	156.0	30	73.9	89.9	80.6	40.5	62.4	81.6
AO-DETR [11]	Swin-L	✓	40	229.0M	156.0	30	74.6 (+0.7)	90.6	81.6	39.3	626	82.2

Table 3: Comparison with state-of-the-art general detectors on OPIXray.

Method	Backbone	MMCL	FPS	PARAMs	GFLOPs	#queries	mAP	FO	ST	SC	UT	MU
Faster R-CNN [38]	ResNeXt-101	*	70	59.83M	28.35	*	73.4	80.6	45.4	89.1	69.1	83.1
MASK R-CNN [39]	ResNeXt-101	*	73	60.04M	28.35	*	77.2	83.6	55.9	89.8	71.5	85.2
Cascade R-CNN [40]	ResNet-50	*	61	68.97M	22.37	*	72.8	75.7	50.0	89.4	70.0	79.0
ATSS [41]	ResNet-101	*	66	51.14M	27.82	*	67.5	72.8	38.0	88.6	58.0	80.2
GFLv1 [42]	ResNeXt-101	*	66	50.70M	28.51	*	75.6	80.0	53.6	89.3	71.7	83.4
Deformable DETR [21]	ResNet-50	✗	60	52.14M	13.47	20	52.4	51.2	21.5	81.6	49.0	58.4
Deformable DETR [21]	ResNet-50	✓	60	52.14M	13.47	20	58.5 (+6.1)	61.5	23.8	85.4	47.8	74.8
RT-DETR [14]	ResNet-50	✗	64	42.81M	17.07	320	61.8	61.1	26.0	88.6	56.4	76.8
RT-DETR [14]	ResNet-50	✓	64	42.81M	17.07	320	62.5 (+0.7)	65.9	22.3	86.4	57.1	80.7
DINO [8]	ResNet-50	✗	54	58.38M	26.89	30	78.2	83.2	58.8	89.4	72.7	86.7
DINO [8]	ResNet-50	✓	54	58.38M	26.89	30	78.6 (+0.4)	83.9	57.2	90.4	74.2	87.1
DINO [8]	Swin-L	✗	40	229.0M	156.0	30	80.8	84.8	63.0	90.1	77.7	88.4
DINO [8]	Swin-L	✓	40	229.0M	156.0	30	81.8 (+1.0)	86.9	64.7	89.8	78.9	88.9
AO-DETR [11]	ResNet-50	✗	54	58.38M	26.89	30	79.2	83.8	60.5	90.1	74.7	87.1
AO-DETR [11]	ResNet-50	✓	54	58.38M	26.89	30	80.3 (+1.1)	84.6	63.6	90.2	74.9	88.0
AO-DETR [11]	Swin-L	✗	40	229.0M	156.0	30	80.8	84.8	63.0	90.1	77.7	88.4
AO-DETR [11]	Swin-L	✓	40	229.0M	156.0	30	82.1 (+1.3)	87.4	63.9	89.9	79.3	89.8

backbones. Similarly, on the OPIXray dataset, as depicted in Table 3, MMCL consistently boosts the detection precision of these models, thereby affirming its versatility and general applicability.

Noteworthily, models with MMCL, compared to the baseline models, show no increase in required GFLOPs and PARAMs during the inference process, and there are no decrease in FPS.

Best model. As presented in Table 2 and Table 3, the implementation of MMCL has propelled AO-DETR (Swin-L) to reach an unprecedented AP of 74.6% on the PIXray dataset and an impressive AP of 82.1% on the OPIXray dataset. This remarkable achievement significantly outperforms a spectrum of models, including those deformable DETR-based models and CNN-based models, showcasing the exceptional efficacy and potential of the MMCL mechanism.

5 Conclusion

We propose a plug-and-play Multi-Class Min-Margin Contrastive Learning (MMCL) mechanism to help Deformable DETR-based models clarify the meaning of content queries, thereby assisting in distinguishing and extracting the semantic features of specific categories from overlapping foreground and background information. Additionally, we have introduced the LIS metric to demonstrate that MMCL can improve the stability of inter-layer label assignment in DETR-like models. Extensive experiments on the X-ray image prohibited items detection datasets PIXray and OPIXray show that MMCL can aid various Deformable DETR-based models in achieving higher accuracy without adding to the computational load of the models.

References

[1] M. Li, B. Ma, H. Wang, D. Chen, and T. Jia, "Gadet: A geometry-aware x-ray prohibited items detector," *IEEE Sensors Journal*, vol. 24, no. 2, pp. 1665–1678, 2024.

[2] C. Zhao, L. Zhu, S. Dou, W. Deng, and L. Wang, "Detecting overlapped objects in x-ray security imagery by a label-aware mechanism," *IEEE Transactions on Information Forensics and Security*, vol. 17, pp. 998–1009, 2022.

[3] A. Chang, Y. Zhang, S. Zhang, L. Zhong, and L. Zhang, "Detecting prohibited objects with physical size constraint from cluttered x-ray baggage images," *Knowledge-Based Systems*, vol. 237, p. 107916, 2022.

[4] L. Zhang, L. Jiang, R. Ji, and H. Fan, "Pidray: A large-scale x-ray benchmark for real-world prohibited item detection," *arXiv preprint arXiv:2211.10763*, 2022.

[5] Y. Wei, R. Tao, Z. Wu, Y. Ma, L. Zhang, and X. Liu, "Occluded prohibited items detection: An x-ray security inspection benchmark and de-occlusion attention module," in *Proceedings of the 28th ACM International Conference on Multimedia*, 2020, pp. 138–146.

[6] N. Carion, F. Massa, G. Synnaeve, N. Usunier, A. Kirillov, and S. Zagoruyko, "End-to-end object detection with transformers," in *European conference on computer vision*. Springer, 2020, pp. 213–229.

[7] S. Liu, F. Li, H. Zhang, X. Yang, X. Qi, H. Su, J. Zhu, and L. Zhang, "Dab-detr: Dynamic anchor boxes are better queries for detr," *arXiv preprint arXiv:2201.12329*, 2022.

[8] H. Zhang, F. Li, S. Liu, L. Zhang, H. Su, J. Zhu, L. M. Ni, and H.-Y. Shum, "Dino: Detr with improved denoising anchor boxes for end-to-end object detection," *arXiv preprint arXiv:2203.03605*, 2022.

[9] Y. Wang, X. Zhang, T. Yang, and J. Sun, "Anchor detr: Query design for transformer-based detector," in *Proceedings of the AAAI conference on artificial intelligence*, vol. 36, no. 3, 2022, pp. 2567–2575.

[10] S. Liu, T. Ren, J. Chen, Z. Zeng, H. Zhang, F. Li, H. Li, J. Huang, H. Su, J. Zhu *et al.*, "Detection transformer with stable matching," in *Proceedings of the IEEE/CVF International Conference on Computer Vision*, 2023, pp. 6491–6500.

[11] M. Li, T. Jia, H. Wang, B. Ma, S. Lin, D. Cai, and D. Chen, "Ao-detr: Anti-overlapping detr for x-ray prohibited items detection," 2024.

[12] L. van der Maaten and G. Hinton, "Visualizing data using t-sne," *Journal of Machine Learning Research*, vol. 9, no. 86, pp. 2579–2605, 2008. [Online]. Available: http://jmlr.org/papers/v9/vandermaaten08a.html

[13] B. Ma, T. Jia, M. Su, X. Jia, D. Chen, and Y. Zhang, "Automated segmentation of prohibited items in x-ray baggage images using dense de-overlap attention snake," *IEEE Transactions on Multimedia*, 2022.

[14] Y. Zhao, W. Lv, S. Xu, J. Wei, G. Wang, Q. Dang, Y. Liu, and J. Chen, "Detrs beat yolos on real-time object detection," *arXiv preprint arXiv:2304.08069*, 2023.

[15] C. Miao, L. Xie, F. Wan, C. Su, H. Liu, J. Jiao, and Q. Ye, "Sixray: A large-scale security inspection x-ray benchmark for prohibited item discovery in overlapping images," in *Proceedings of the IEEE/CVF conference on computer vision and pattern recognition*, 2019, pp. 2119–2128.

[16] N. Otsu, "A threshold selection method from gray-level histograms," *IEEE Transactions on Systems, Man, and Cybernetics*, vol. 9, no. 1, pp. 62–66, 1979.

[17] D. Jia, Y. Yuan, H. He, X. Wu, H. Yu, W. Lin, L. Sun, C. Zhang, and H. Hu, "Detrs with hybrid matching," in *Proceedings of the IEEE/CVF Conference on Computer Vision and Pattern Recognition*, 2023, pp. 19 702–19 712.

[18] Z. Hu, Y. Sun, J. Wang, and Y. Yang, "Dac-detr: Divide the attention layers and conquer," *Advances in Neural Information Processing Systems*, vol. 36, 2024.

[19] Z. Zong, G. Song, and Y. Liu, "Detrs with collaborative hybrid assignments training," in *Proceedings of the IEEE/CVF international conference on computer vision*, 2023, pp. 6748–6758.

[20] Q. Chen, X. Chen, J. Wang, S. Zhang, K. Yao, H. Feng, J. Han, E. Ding, G. Zeng, and J. Wang, "Group detr: Fast detr training with group-wise one-to-many assignment," in *Proceedings of the IEEE/CVF International Conference on Computer Vision*, 2023, pp. 6633–6642.

[21] X. Zhu, W. Su, L. Lu, B. Li, X. Wang, and J. Dai, "Deformable {detr}: Deformable transformers for end-to-end object detection," in *International Conference on Learning Representations*, 2021. [Online]. Available: https://openreview.net/forum?id=gZ9hCDWe6ke

[22] T. Chen, S. Kornblith, M. Norouzi, and G. Hinton, "A simple framework for contrastive learning of visual representations," in *Proceedings of the 37th International Conference on Machine Learning*, ser. Proceedings of Machine Learning Research, H. D. III and A. Singh, Eds., vol. 119. PMLR, 13–18 Jul 2020, pp. 1597–1607. [Online]. Available: https://proceedings.mlr.press/v119/chen20j.html

[23] K. He, H. Fan, Y. Wu, S. Xie, and R. Girshick, "Momentum contrast for unsupervised visual representation learning," in *Proceedings of the IEEE/CVF conference on computer vision and pattern recognition*, 2020, pp. 9729–9738.

[24] Y. Li, P. Hu, Z. Liu, D. Peng, J. T. Zhou, and X. Peng, "Contrastive clustering," in *Proceedings of the AAAI conference on artificial intelligence*, vol. 35, no. 10, 2021, pp. 8547–8555.

[25] Y. Li, M. Yang, D. Peng, T. Li, J. Huang, and X. Peng, "Twin contrastive learning for online clustering," *International Journal of Computer Vision*, vol. 130, no. 9, pp. 2205–2221, 2022.

[26] F. Schroff, D. Kalenichenko, and J. Philbin, "Facenet: A unified embedding for face recognition and clustering," in *Proceedings of the IEEE conference on computer vision and pattern recognition*, 2015, pp. 815–823.

[27] F. Wang, J. Cheng, W. Liu, and H. Liu, "Additive margin softmax for face verification," *IEEE Signal Processing Letters*, vol. 25, no. 7, pp. 926–930, 2018.

[28] Y. Sun, C. Cheng, Y. Zhang, C. Zhang, L. Zheng, Z. Wang, and Y. Wei, "Circle loss: A unified perspective of pair similarity optimization," in *Proceedings of the IEEE/CVF conference on computer vision and pattern recognition*, 2020, pp. 6398–6407.

[29] P. Khosla, P. Teterwak, C. Wang, A. Sarna, Y. Tian, P. Isola, A. Maschinot, C. Liu, and D. Krishnan, "Supervised contrastive learning," *Advances in neural information processing systems*, vol. 33, pp. 18 661–18 673, 2020.

[30] S. Chopra, R. Hadsell, and Y. LeCun, "Learning a similarity metric discriminatively, with application to face verification," in *2005 IEEE Computer Society Conference on Computer Vision and Pattern Recognition (CVPR'05)*, vol. 1, 2005, pp. 539–546 vol. 1.

[31] J. Xie, J. Xiang, J. Chen, X. Hou, X. Zhao, and L. Shen, "Contrastive learning of class-agnostic activation map for weakly supervised object localization and semantic segmentation," 2022.

[32] F. Li, H. Zhang, S. Liu, J. Guo, L. M. Ni, and L. Zhang, "Dn-detr: Accelerate detr training by introducing query denoising," in *Proceedings of the IEEE/CVF Conference on Computer Vision and Pattern Recognition*, 2022, pp. 13 619–13 627.

[33] R. Girshick, J. Donahue, T. Darrell, and J. Malik, "Region-based convolutional networks for accurate object detection and segmentation," *IEEE transactions on pattern analysis and machine intelligence*, vol. 38, no. 1, pp. 142–158, 2015.

[34] Z. Liu, Y. Lin, Y. Cao, H. Hu, Y. Wei, Z. Zhang, S. Lin, and B. Guo, "Swin transformer: Hierarchical vision transformer using shifted windows," in *Proceedings of the IEEE/CVF international conference on computer vision*, 2021, pp. 10 012–10 022.

[35] K. Chen, J. Wang, J. Pang, Y. Cao, Y. Xiong, X. Li, S. Sun, W. Feng, Z. Liu, J. Xu, Z. Zhang, D. Cheng, C. Zhu, T. Cheng, Q. Zhao, B. Li, X. Lu, R. Zhu, Y. Wu, J. Dai, J. Wang, J. Shi, W. Ouyang, C. C. Loy, and D. Lin, "MMDetection: Open mmlab detection toolbox and benchmark," *arXiv preprint arXiv:1906.07155*, 2019.

[36] J. Deng, W. Dong, R. Socher, L.-J. Li, K. Li, and L. Fei-Fei, "Imagenet: A large-scale hierarchical image database," in *2009 IEEE conference on computer vision and pattern recognition*. Ieee, 2009, pp. 248–255.

[37] K. He, X. Zhang, S. Ren, and J. Sun, "Deep residual learning for image recognition," in *Proceedings of the IEEE conference on computer vision and pattern recognition*, 2016, pp. 770–778.

[38] S. Ren, K. He, R. Girshick, and J. Sun, "Faster r-cnn: Towards real-time object detection with region proposal networks," *IEEE Transactions on Pattern Analysis & Machine Intelligence*, vol. 39, no. 06, pp. 1137–1149, 2017.

[39] K. He, G. Gkioxari, P. Dollár, and R. Girshick, "Mask r-cnn," in *Proceedings of the IEEE international conference on computer vision*, 2017, pp. 2961–2969.

[40] Z. Cai and N. Vasconcelos, "Cascade r-cnn: Delving into high quality object detection," in *Proceedings of the IEEE Conference on Computer Vision and Pattern Recognition (CVPR)*, June 2018.

[41] S. Zhang, C. Chi, Y. Yao, Z. Lei, and S. Z. Li, "Bridging the gap between anchor-based and anchor-free detection via adaptive training sample selection," in *Proceedings of the IEEE/CVF conference on computer*

vision and pattern recognition, 2020, pp. 9759–9768.

[42] X. Li, W. Wang, L. Wu, S. Chen, X. Hu, J. Li, J. Tang, and J. Yang, "Generalized focal loss: Learning qualified and distributed bounding boxes for dense object detection," *Advances in Neural Information Processing Systems*, vol. 33, pp. 21 002–21 012, 2020.

A Explore the significance of clarifying the category meaning of the content queries:

In this part, we analyze the role of content queries in the decoder of models based on deformable DETR, and then elucidate why we engage in contrastive learning for content queries according to the number of categories. Given an image, the backbone and encoder extract the mulit-scale spatial feature $X \in \mathbb{R}^{N \times C}$, and predict a group of proposals including classification results C and localization results $R \in \mathbb{R}^{N \times 4}$. Taking the decoder's match part of DINO as an example, in a two-stage approach, the top N_{pred} localization results with the highest classification confidence predicted by the encoder are used as reference boxes $R^0 \in \mathbb{R}^{N_{pred} \times 4}$, where N_{pred} is the same as the number of queries. Positional queries $Q_q^0 \in \mathbb{R}^{N_{pred} \times C}$ are obtained using positional encoding[8], represented as $Q_q^0 = PE(R^0)$, and content queries $Q_c^0 \in \mathbb{R}^{N_{pred} \times C}$ is randomly initialized, represented as $Q_c^0 =$ Embedding(N_{pred}, C). The decoder is then responsible for further feature extraction from X with reference boxes and query pairs by L decoder blocks, which includes self-attention, deformable attention, and linear mapping layers, to predict the final results.

Self-attention combines the content query and positional query by element-wise addition to form the final query, which is then used to establish a global self-attention map to extract the content of the content query, updating and optimizing it. The process of self-attention can be represented as follows:

$$Q_{s,c}^l = \mathcal{D}_s^l(Q_s^l, K_s^l, V_s^l; \theta_s^l), \quad Q_s^l = K_s^l = Q_c^l + Q_q^l, \quad V_s^l = Q_c^l \tag{7}$$

where $\mathcal{D}_s^l$ represents the self-attention mechanism of the l-th decoder block. $l \in \{x \mid x \in \mathbb{Z}, 0 \leq x < L\}$, represents the decoder block index, and $L = 6$ denotes the total number of decoder blocks. Subscript s, c, and p and mean the self-attention, the content embedding and the position embedding. The K, V, θ are the key, value, parameters, respectively.

Deformable attention uses reference boxes R^l to assist the query in capturing image features X, outputing the queries $Q_{d,c}^{l+1}$ which is more suitable for the final prediction. The process can be denoted as follows:

$$Q_c^{l+1} = Q_{d,c}^{l+1} = \mathcal{D}_d^l(Q_d^l, R^l, X; \theta_d^l), \quad Q_d^l = Q_{s,c}^l + Q_q^l, \tag{8}$$

where $\mathcal{D}_d^l$ represents the deformable attention mechanism of the l-th decoder block. The subscript d means the deformable attention.

Finally, the linear mapping layers $\mathcal{L}_{R,C}^l$ of the decoder will utilize Q_c^{l+1} to predict deviations ΔR^{l+1} and classification results C^{l+1}, expressed as follows:

$$R^{l+1} = \sigma(\sigma^{-1}(R^l) + \Delta R^{l+1}), \quad \{\Delta R^{l+1}, C^{l+1}\} = \mathcal{L}_{R,C}^l(Q_c^{l+1}), \tag{9}$$

where $\sigma(\cdot)$ and $\sigma^{-1}(\cdot)$ denote the sigmoid and inverse sigmoid functions, respectively.

Overall, the decoder block of the l-th layer can be simplified as follows:

$$Q_c^{l+1}, R^{l+1}, C^{l+1} = \mathcal{D}^l(Q_c^l, R^l, X; \theta^l) \tag{10}$$

From the aforementioned process, it can be observed that content queries provide direct information for classification and localization, whereas positional queries primarily assist in delivering prior knowledge of positioning. Therefore, theoretically, if we can decouple various potential semantic features of categories in content queries and retain the semantic features of one category, then its detection capability for items of that category will be enhanced.

B Prediction Results Visualization

Fig. 5 illustrates some visualization of detection results on the PIXray dataset, comparing the performance of the DINO model before and after the integration of the MMCL.

In some special detection scenarios, the model with MMCL can more effectively detect true positives (TPs), such as successfully detecting darts in group (b) and scissors in group (c). This indicates that MMCL enhances the recall rate (TP/P) of model.

In some complex detection scenarios, the baseline model may miss some targets (generating false negatives, FNs) and produce false positives (FPs). For example, in group (d), the baseline model not only fails to detect the hammer but also mistakenly identifies the scissors as pliers. In contrast, the model with MMCL can achieve accurate classification results and ground truth boxes, indicating that MMCL reduces the miss rate (FN/P) of model.

In summary, the visualization results demonstrate that our MMCL mechanism enhances the detection performance of DETR-like models on X-ray images with overlapping phenomena, thereby fully validating the effectiveness of our proposed method.

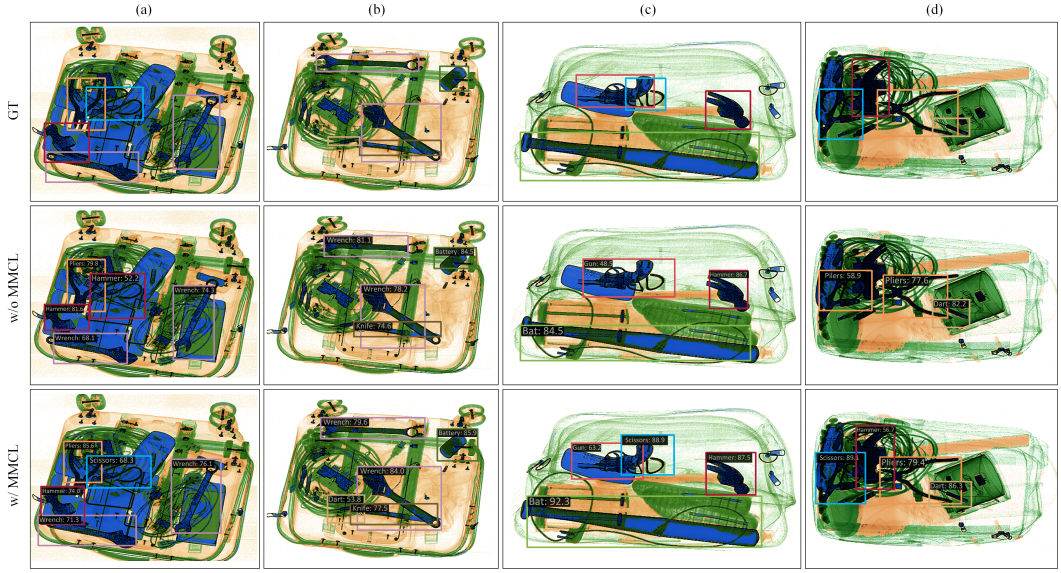

Figure 5: The visualization of some prediction results.

C Visualization of Sampling Points

Fig. 6 illustrates the detailed visualization of the sampling points in the 4-th decoder layer of the DINO model,both before and after the integration of MMCL. The PIXray dataset consists of 15 categories, and we set the number of queries to 30. We take the bat, wrench and gun, which are three prohibited items with different shapes, as examples. After integrating MMCL, their corresponding content query group indexes are the 2-nd, 11-th and 12-th groups. For clarity, we select the 4-th, 23-rd and 25-th queries from each group and visualize their sampling points to deeply analyze the changes in the category attributes of the content queries before and after the integration of MMCL.

In group (a), the 4-th query of the baseline model does not have a fixed category attribute, so it has no objects detected in Img A and Img B, but detect the bat in Img C. However, when MMCL is integrated, the category attribute of the 4-th query is determined to be the bat, so the query only detects the bat in the image. Since there is no bat in Img A, the 4-th query has no objects detected.

In group (b), the category attribute of the 23-rd query in the baseline model is the gun in Img A, does not detect any objects in Img B, and changes to the bat in Img C, indicating that the category attribute of the query is not fixed. However, when MMCL is integrated, the category attribute of the 23-rd query is determined to be the wrench, so it only detects the wrench in Img A, Img B and Img C.

In group (c), the category attribute of the 25-th query in the baseline model is the gun in Img A and the wrench in Img C. After integrating MMCL, the category attribute of the 25-th query in the model is the gun, so the sampling point successfully notices the gun in Img A and Img B.

Overall, the category attribute of the query in the baseline model is not fixed, but after integrating MMCL, the probability of the query detecting a certain fixed category significantly increases, thereby improving the detection performance of the model. This analysis illustrates the impact of MMCL on model performance and its potential in improving the stability of query category attributes.

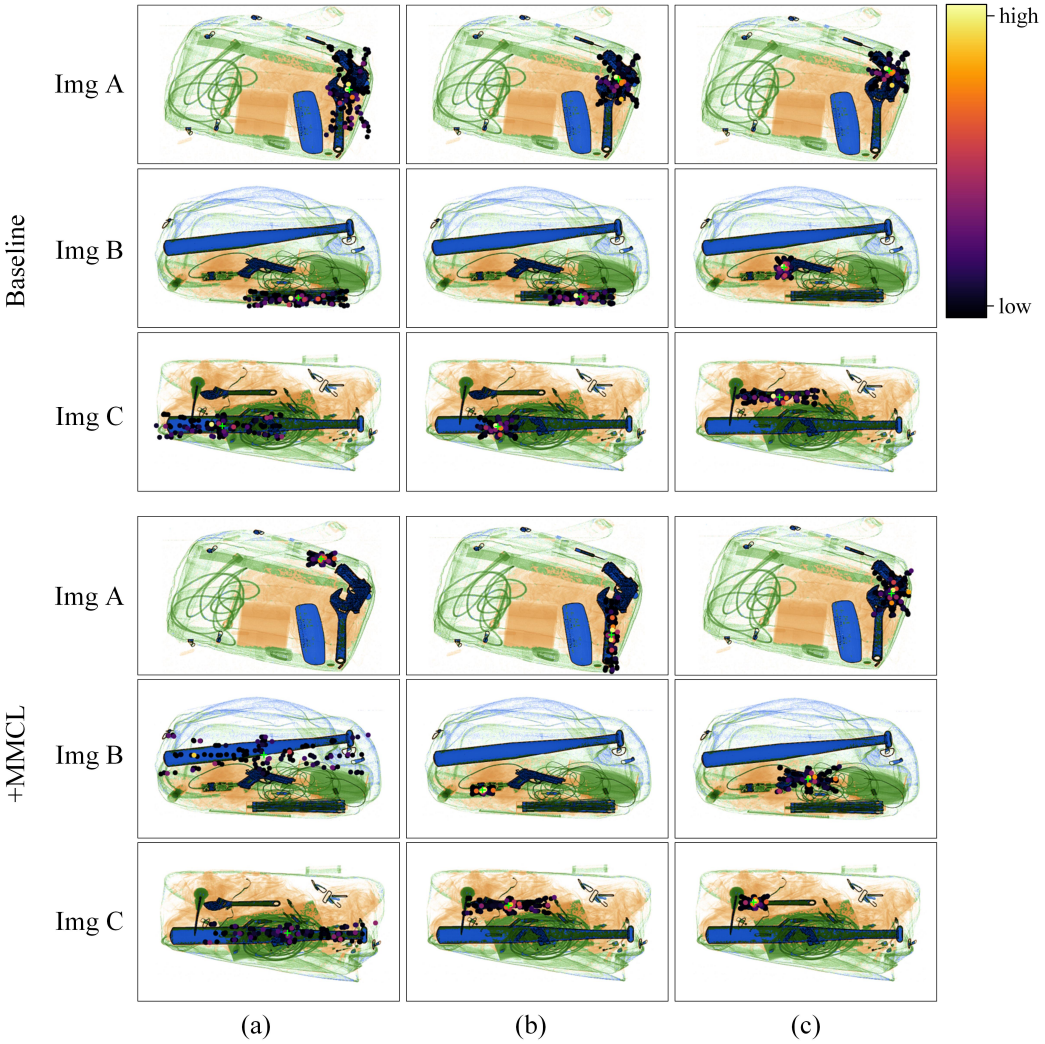

Figure 6: The visualization of some sampling points. We selected the query from the 4-th layer of the decoder to analyze its category attributes. In this context, group(a) represents the 4-th query, group(b) represents the 23-rd query, and group(c) represents the 25-th query.